An efficient Born normal mode method to compute sensitivity kernels and synthetic seismograms in the Earth

Y Capdeville

Geophys. J. Int. (2005) **163,** 639–646 doi: 10.1111/j.1365-246X.2005.02765.x

An efficient Born normal mode method to compute sensitivity kernels and synthetic seismograms in the Earth

Y. Capdeville

Departement de sismologie, Institut de Physique du Globe de Paris, Paris, France. E-mail: capdevil@ipgp.jussieu.fr

Accepted 2005 July 28. Received 2005 July 21; in original form 2005 January 14

SUMMARY

We present an alternative to the classical mode coupling method scheme often used in global seismology to compute synthetic seismograms in laterally heterogeneous earth model and Frechet derivatives for tomographic inverse problem with the normal modes first-order Born approximation. We start from the first-order Born solution in the frequency domain and we use a numerical scheme for the volume integration, which means that we have to compute the effect of a finite number of scattering points and sum them with the appropriate integration weight. For each scattering point, 'source to scattering point' and 'scattering point to receivers' expressions are separated before applying a Fourier transform to return to the time domain. Doing so, the perturbed displacement is obtained, for each scattering point, as the convolution of a forward wavefield from the source to the scattering point with a backward wavefield from the scattering integration point to the receiver. For one scattering point and for a given number of time steps, the numerical cost of such a scheme grows as (number of receivers + the number of sources) $\times$ (corner frequency)^2 to be compared to (number of receivers $\times$ the number of sources) $\times$ (corner frequency)^4 when the classical normal mode coupling algorithm is used. Another interesting point is, when used for Frechet kernel, the computing cost is (almost) independent of the number of parameters used for the inversion. This algorithm is similar to the one obtained when solving the adjoint problem. Validation tests with respect to the spectral element method solution both in the Frechet derivative case and as a synthetic seismogram tool shows a good agreement. In the latter case, we show that non-linearity can be significant even at long periods and when using existing smooth global tomographic models.

Key words: Fréchet derivatives, Global seismology, normal modes.

1 INTRODUCTION

The normal mode solution of the wave equation is well known and widely used in global seismology when dealing with spherically symmetric models in the 20 s and longer period range. When dealing with laterally heterogeneous models, a standard method is the first-order perturbation of the normal mode basis obtained in a spherically symmetric reference earth model. This approximation is only valid for weak enough lateral heterogeneities and for short enough time-series. This 'weak enough' condition, which is closely related to the 'short enough' time condition, is not clearly defined and should be checked in each particular situation. Most of the long wavelength global tomographic models are based on methods derived from the Born solution in the normal modes framework. The computations involve the coupling of the modes obtained in the spherically symmetric reference model due to the 3-D structure. Depending on the roughness of the 3-D model and of the corner frequency of the source, the number of modes that need to be coupled can be very large and, therefore, computationally intensive. In result,the complete Born solution is rarely used and less computationally intensive methods based on approximations to the Born approximation have been developed for practical uses. Among incremental approximations to the Born approximation, we can quote the very popular 'path average' approximation (Woodhouse & Dziewonski 1984) in which perturbations due to the average spherically symmetric model on the source–receiver path is taken into account. This approximation provides only 1-D sensitivity kernels, but is very efficient. A better approximation is NACT (Li & Tanimoto 1993; Li & Romanowicz 1995), an asymptotic method, in which is included the cross coupling between different dispersion branches and provides 2-D sensitivity kernels. These different approximations are very interesting because their efficiency allows one to compute the large number of synthetic seismograms required for tomography in a acceptable CPU time. It is nevertheless interesting to go beyond these approximations and use the full Born approximation to include effects such as focusing or component conversions due to lateral heterogeneities. In this paper we present an efficient normal mode Born technique in which the full mode coupling is present but not explicitly. In this approach, lateral heterogeneities (of a model for synthetic seismograms, or of a spatial parameter for Frechet kernels) are discretized

as a finite number of scattering points over an integration mesh. The perturbation (or partial derivative) of displacement due to a lateral heterogeneity is computed with the convolution of a direct wavefield from the source to a scattering point with a backward wavefield for the receiver to the scattering point. This scheme is significantly more efficient than the explicit mode coupling solution and does not require to specify an angular coupling range Δl as it is usually the case. This solution is equivalent to the one obtained when solving the adjoint problem (e.g. Lailly 1983; Tarantola 1984, 1988; Mora 1987; Geller & Hara 1993; Pratt *et al.* 1998; Tromp *et al.* 2005) and similar to the one used by Tanimoto (1990) for surface waves on a membrane.

We will first introduce the classical mode coupling approach and then focus on this alternative approach. We will then present practical and numerical considerations before presenting some validation tests with respect to the spectral element Method (SEM) solution.

2 THEORY

Let us first introduce some notations that will be used in that paper, such as the dot product:

$$\mathbf{u}\cdot\mathbf{v}=\sum_{i=1,3}u_i v_i\,, \tag{1}$$

and the inner product

$$(\mathbf{u},\mathbf{v})=\int_V \mathbf{u}^*(\mathbf{r})\cdot\mathbf{v}(\mathbf{r})\,d\mathbf{r}\,, \tag{2}$$

where * denotes the complex conjugate and V the earth volume.

The displacement $\mathbf{u}$ in the Earth has to be solution of the following wave equation

$$\boldsymbol{\mathcal{L}}\mathbf{u}=\mathbf{f}, \tag{3}$$

where $\mathbf{f}$ is the external source term which represent the earthquake and $\mathcal{L}$ is the anelasto-dynamic operator. In the frequency domain,

$$\boldsymbol{\mathcal{L}}\mathbf{u}=-\omega^2\rho\mathbf{u}+\boldsymbol{\mathcal{A}}\mathbf{u}, \tag{4}$$

where $\boldsymbol{\mathcal{A}}$ is the anelatic operator and ρ is the density. In the following, we will assume that the external source $\mathbf{f}$ is a point source in space located at $\mathbf{r}_s$ and a step function in time.

We consider $\boldsymbol{\mathcal{L}}=\boldsymbol{\mathcal{L}}_0+\delta\boldsymbol{\mathcal{L}}$, where $\boldsymbol{\mathcal{L}}_0$ is the anelasto-dynamic operator in a reference earth model and $\delta\boldsymbol{\mathcal{L}}$ a perturbation with respect to $\boldsymbol{\mathcal{L}}_0$. For the sake of simplicity, only perturbation of the anelastic tensor will be considered and, therefore, $\delta\boldsymbol{\mathcal{L}}=\delta\boldsymbol{\mathcal{A}}$.The density perturbation can nevertheless be included with no extra difficulties and practical expressions including density effect are given in Appendix A. Because the normal mode solution is well known in spherically symmetric models, the reference model is often (if not always) chosen spherically symmetric for the normal mode perturbation scheme. The displacement wavefield is also written under the form $\mathbf{u}=\mathbf{u}_0+\delta\mathbf{u}$, where $\boldsymbol{\mathcal{L}}_0\mathbf{u}_0=\mathbf{f}$ and, to the first order, it can be easily shown that

$$\boldsymbol{\mathcal{L}}_0\delta\mathbf{u}=-\delta\boldsymbol{\mathcal{L}}\mathbf{u}_0. \tag{5}$$

We name $\mathbf{u}_K$ and ω_k the set of eigenfunctions and eigenfrequencies, solutions of $\boldsymbol{\mathcal{L}}_0\mathbf{u}=0$ with the index $k=(q,n,l)$ and $K=(k,m)$, where q can take two values, one for spheroidal modes and one for toroidal modes, n is the radial order, l the angular order and m the azimuthal order. Because of the spherical symmetry of the reference model, the eignefrequencies ω_k do not depend on the azimuthal order.

The first-order perturbation displacement wavefield expression in the frequency domain is (Woodhouse 1983; Tanimoto 1984),

$$\delta\mathbf{u}(\mathbf{r}_r,\omega)\cdot\mathbf{v}=-\sum_{KK'}\int_V\frac{R_K L_{KK'}(\mathbf{r})S_{K'}}{i\omega\left(\omega_k^2-\omega^2\right)\left(\omega_{k'}^2-\omega^2\right)}\,d\mathbf{r}, \tag{6}$$

where $R_K=\mathbf{u}_K(\mathbf{r}_r)\cdot\mathbf{v}$ is the receiver term for component $\mathbf{v}$, $S_K=(\mathbf{u}_K,\mathbf{f})$ the source term and

$$L_{KK'}(\mathbf{r})=\mathbf{u}_K^*(\mathbf{r})\cdot\delta\boldsymbol{\mathcal{L}}(\mathbf{r})\mathbf{u}_{K'}(\mathbf{r})\,. \tag{7}$$

We will first explain how, starting from eq. (6), $\delta\mathbf{u}(\mathbf{r}_r,t)$ is usually computed in seismology, and then we will propose an alternative.

2.1 A classical way

Performing an inverse Laplace–Fourier transform of eq. (6), we obtain

$$\delta\mathbf{u}(\mathbf{r}_r,t)\cdot\mathbf{v}=\sum_{KK'}g_{kk'}(t)\int_V R_K L_{KK'}(\mathbf{r})S_{K'}\,d\mathbf{r}\,, \tag{8}$$

with

$$g_{kk'}(t)=\frac{\omega_{k'2}[1-\cos(\omega_k t)][1-\cos(\omega_{k'}t)]}{\omega_k^2\omega_{k'2}(\omega_k^2-\omega_{k'2})}H(t)\,. \tag{9}$$

When $k=k'$ in the previous equation, a first-order Taylor expansion has to be performed on $g_{kk'}$, which results in a term proportional to time t (secular term). To compute the volume integral in eq. (8), two approaches have been considered. In the first one, the lateral heterogeneities are expanded over the spherical harmonics basis (e.g. Woodhouse & Dahlen 1978; Woodhouse & Girnius 1982; Tanimoto 1986), which allows the horizontal part of the volume integral to be computed analytically using Wigner 3-j symbols (Edmonds 1960), or asymptotically, using the stationary phase approximation (Romanowicz 1987). In the second approach, (e.g. Snieder 1986; Snieder & Romanowicz 1988; Li & Tanimoto 1993; Capdeville *et al.* 2000) the volume integral of eq. (8) is performed numerically and it can be seen as a sum over a finite number of scattering points. R_K, S_K and $L_{KK'}$ are usually expanded over the generalized spherical harmonics basis (Phinney & Burridge 1973), and using the generalized spherical harmonics summation theorem, the sum over m can be suppressed to reduce the amount of computing. In practice, synthetic seismograms are only computed down to a given corner frequency, which makes it possible to define a maximum angular degree $l_{\max}$ up to which the sum over k and k' must be computed. Knowing that the number of eigenfrequencies below the corner frequency of the source is proportional to $l_{\max}^2$, for a single integration point, the number of floating point operation grows as $l_{\max}^4$ as the corner frequency increases if all the modes are coupled. In practice, not all mode couplings are considered, which reduces the number of computations but also reduces the accuracy. These computations have to be performed for each pair of source and receiver, therefore the numerical cost for a single scattering point increase as $N_s\times N_r\times l_{\max}^4$, where N_r and N_s are the number of receivers and sources, respectively.

2.2 An alternative to the classical way

In the rest of this article, we will use a numerical integration scheme to compute the volume integral of eq. (6). Using the definition of

$L_{KK'}$, eq. (6) can be rewritten as

$$\delta\mathbf{u}(\mathbf{r}_r,\omega)\cdot\mathbf{v} = -\int_V \left[\sum_K \frac{\mathbf{u}_K^*(\mathbf{r})R_K}{(\omega_k^2-\omega^2)}\right]\cdot\delta\boldsymbol{\mathcal{L}}(\mathbf{r})\left[\sum_K \frac{\mathbf{u}_K(\mathbf{r})S_K}{i\omega(\omega_k^2-\omega^2)}\right]d\mathbf{r}, \quad (10)$$

and in the time domain

$$\delta\mathbf{u}(\mathbf{r}_r,t)\cdot\mathbf{v} = -\int_V\int \mathbf{B}(\mathbf{r},\tau)\cdot\delta\boldsymbol{\mathcal{L}}(\mathbf{r})\boldsymbol{F}(\mathbf{r},\tau-t)\,d\tau\,d\mathbf{r}\,, \quad (11)$$

where

$$\mathbf{B}(\mathbf{r},t) = \sum_K \mathbf{u}_K^*(\mathbf{r})R_K\frac{\sin(\omega_k t)}{\omega_k}H(t)\,, \quad (12)$$

and

$$\mathbf{F}(\mathbf{r},t) = \sum_K \mathbf{u}_K(\mathbf{r})S_K\frac{1-\cos(\omega_k t)}{\omega_k^2}H(t)\,, \quad (13)$$

where H is the Heaviside function. We therefore have, for each integration point, a convolution of a forward wavefield (**F**) from the source to the scattering point and a backward wavefield (**B**) from the receiver to the scattering point. For each scattering point of the integration mesh, the **B** and **F** fields can be computed independently for each source and receiver. Therefore, for a single scattering point and for a constant number of time steps, the number of computations increases as $(N_s+N_r)\times l_{\max}^2$, which make this process numerically more interesting than eq. (8). A practical expression of eq. (11) is derived in appendix A.

The same result can be obtained directly starting form eq. (5). We name $\mathbf{G}(\mathbf{r};\mathbf{r}_s,t)$ the Green's function solution of

$$\boldsymbol{\mathcal{L}}_0\mathbf{u}(\mathbf{r},t) = \delta(\mathbf{r}_s-\mathbf{r})\delta(t)\mathbf{I}\,, \quad (14)$$

where **I** is the identity tensor. Noting that eq. (5) is the same as eq. (14) with a different source term, we obtain:

$$\delta\mathbf{u}(\mathbf{r}_r,t) = -\int_V\int \mathbf{G}(\mathbf{r}_r;\mathbf{r},\tau)\cdot\delta\boldsymbol{\mathcal{L}}\mathbf{u}_0(\mathbf{r},t-\tau)\,d\tau\,d\mathbf{r}\,, \quad (15)$$

which is equivalent to eq. (11). This result is also equivalent to the one obtained when solving the adjoint problem (Lailly 1983; Tarantola 1984, 1988; Mora 1987; Pratt *et al.* 1998; Tromp *et al.* 2005).

3 NUMERICAL CONSIDERATIONS

3.1 Sum truncations

Sums over k of eqs (12) and (13) cannot be computed numerically without truncations. Indeed, index k is a summary of indexes q, n and l. q can only take two values but both the radial order n and angular l order lie in $[0,+\infty[$. In practical cases, the source term has a corner frequency ω_c or the signal will be filtered with a filter with a corner frequency ω_c. In that case, time expressions eqs (12) and (13) have to be rewritten to allow sum truncations with an acceptable accuracy. Here we will present in detail the case of the time expression in eq. (12), but a similar operation can be performed for eq. (13) with little differences. The $\frac{\sin(\omega_k t)}{\omega_k}H(t)$ in eq. (12) has been obtained with the Fourier transformation of

$$h_k(\omega) = \frac{1}{\omega_k^2-\omega^2} = \frac{1}{2\omega_k^2}\left(\frac{1}{\omega_k-\omega}+\frac{1}{\omega_k+\omega}\right). \quad (16)$$

Using the Cauchy theorem, it can easily shown that

$$\int_{-\infty}^{+\infty} h_k(\omega)e^{-i\omega t}d\omega = \frac{\sin\omega_K t}{\omega_k}H(t)\,. \quad (17)$$

Now, either because $h_k(\omega)$ is multiplied by a source term that has a corner frequency or either because numerical computation will stop at the Nyquist frequency, $h_k(\omega)$ is always multiplied by a function $f(\omega)$ with a given corner frequency ω_c. Even if it is often done in practice, we do not have

$$\int_{-\infty}^{+\infty} h_k(\omega)f(\omega)e^{-i\omega t}d\omega = f(\omega_k)\frac{\sin\omega_k t}{\omega_k}H(t)\,. \quad (18)$$

Indeed, eq. (18) is true only if $f(\omega)e^{-i\omega t}$ can be extended to an analytic complex function on the entire complex plane, which is not the case for most of the usual bounded filters with a frequency cut-off. In general, we have

$$\int_{-\infty}^{+\infty} h_k(\omega)f(\omega)e^{-i\omega t}d\omega = {}_f h_k^{(1)}(t) + {}_f h_k^{(2)}(t)\,, \quad (19)$$

with

$${}_f h_k^{(1)}(t) = f(\omega_k)\frac{\sin\omega_k t}{\omega_k}H(t)\,, \quad (20)$$

and

$${}_f h_k^{(2)}(t) = \int_{-\infty}^{+\infty}\frac{1}{2\omega_k^2}\left(\frac{f(\omega)-f(\omega_k)}{\omega_k-\omega}+\frac{f(\omega)-f(-\omega_k)}{\omega_k+\omega}\right)e^{-i\omega t}d\omega\,. \quad (21)$$

The distribution of eigenfrequencies (an example is given Fig. 1) allows, for a given corner frequency, to determine a maximum angular degree $l_{\max}$ and for each l a maximum radial order $n_{\max}(l)$ after which ${}_f h_k^{(1)}$ terms are always equal to zero. This is not the case for terms ${}_f h_k^{(2)}$, even if it decays rapidly for (l,n) outside of $[0,l_{\max}]\times[0,n_{\max}(l)]$. A practical solution is to take an $[0,l]\times[0,n]$ window bigger than $[0,l_{\max}]\times[0,n_{\max}(l)]$ with a taper weighting of terms outside of $[0,l_{\max}]\times[0,n_{\max}(l)]$. This is nevertheless an approximation that introduce errors that depend on the source, heterogeneities and receiver geometrical configurations.

In classical approaches ${}_f h_k^{(2)}$ can be often neglected because it has an effect only near $t=0$. In our case, when the scattering point is close to the source or to the receiver, the influence of the second term becomes very important around $t=0$ for one of the two fields **F** or **B**. Because of the convolution, this error is spread to the whole signal as it can be seen on the example given in Fig. 2. In a realistic application there are always lateral heterogeneities around the source and the receiver. Neglecting ${}_f h_k^{(2)}$ using the approach presented in

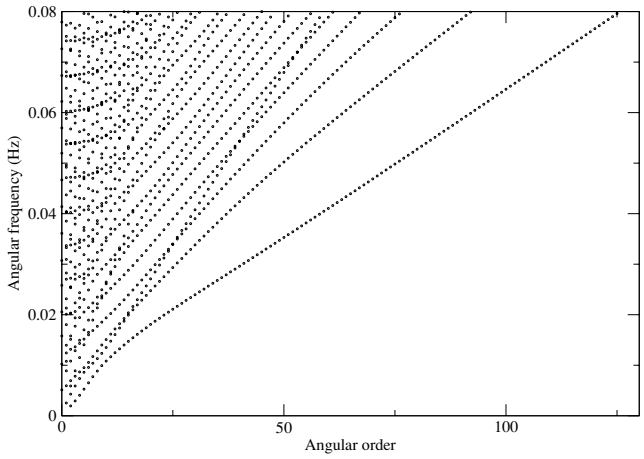

Figure 1. Some Rayleigh eigenfrequencies in PREM (Dziewonski & Anderson 1981).

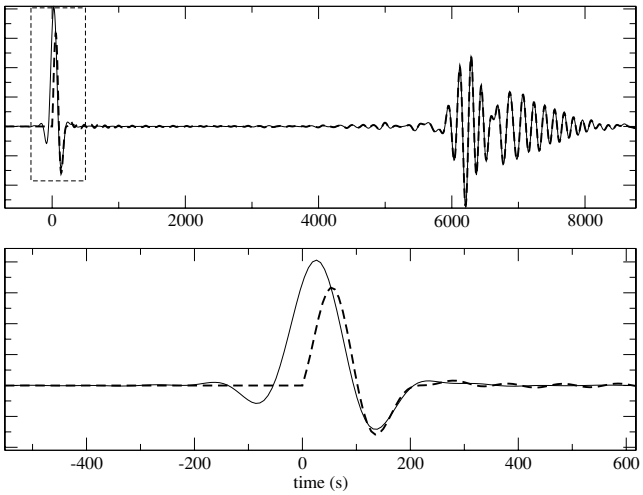

Figure 2. Forward term **F** (13) computed for a Dirac source time function for a scattering point at less than a degree from the source. The filter f is cosine filter with a taper from 200 s to 80 s. In dotted line is plotted the result obtained when only ${}_f h_k^1$ of eq. (19) is used and in plain line is plotted the result obtained when both terms of eq. (19) are used. The lower plot is a zoom around the origin time of the upper plot. One can see that including ${}_f h_k^2$ terms indeed affects only the early time on the trace, but the effect is significant around $t = 0$. Taking into account this effect is important to obtain a good result when convolution eq. (11).

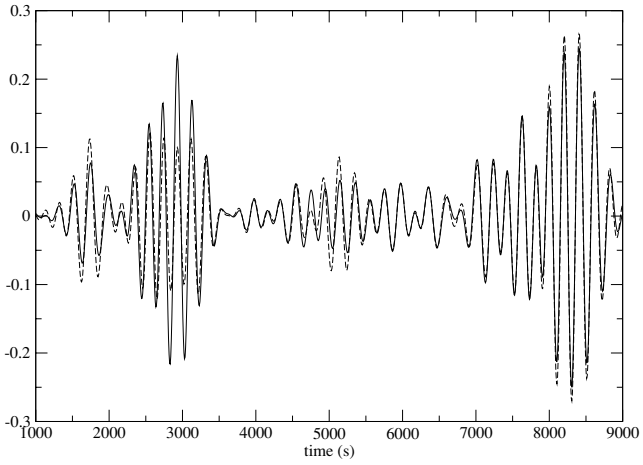

Figure 3. Differential traces (difference between traces computed in the 3-D model model and traces computed in the 1-D reference model) computed with (solid line) and without (dotted line) the terms ${}_f h_k^2$ and ${}_b h_k^2$ in the 3-D tomographic SAW24B16 model for an epicentral distance of 70 degree along the equator. The source has 150 s corner frequency, a depth of 19 km and an origin time at 1000 s. The effect of neglecting ${}_f h_k^{(2)}$ can be important especially for the R1 scattered train (around 3000 s)

this paper can be an important issue, knowing that the scattered wavefield is especially sensitive to structure below the source and below the receiver. An example of the effect of neglecting ${}_f h_k^{(2)}$ in the 3-D tomographic model SAW24B16 (Mégnin & Romanowicz 2000) is given Fig. 3.

3.2 Integration mesh

The volume integral of eq. (11) needs to be computed numerically. In order to do so, we use here the same integration scheme as the one used to solve the wave equation at the global scale with the SEM (Chaljub 2000; Chaljub *et al.* 2003). An example of such a mesh is given in Fig. 4. Many other choices for this numerical integration could have been made, but the availability of this integration scheme and also the good accuracy with no over sampling at the poles justify this choice. The sphere is first divided into N_e non-overlapping deformed cubic elements. The 'cubic sphere' proposed by Sadourny (1972) and further extended by Ronchi *et al.* (1996) allows such a meshing of a spherical surface by decomposing it into six regions of identical shape, which can be mapped onto a cube face. To obtain the meshing of a spherical shell, spherical surfaces are connected radially. In each element, the numerical integration is performed using the Gauss–Lobatto–Legendre (GLL) quadrature in each Cartesian direction. In each of these Cartesian direction, the polynomial basis of degree N is built using the Lagrange polynomial associated with GLL points. If we name

$$\mathbf{d}(\mathbf{r}) = \int \mathbf{B}(\mathbf{r}, \tau) \cdot \delta\boldsymbol{\mathcal{L}}(\mathbf{r}) \boldsymbol{F}(\mathbf{r}, \tau - t)\, d\tau \,, \tag{22}$$

then numerical approximation of eq. (11) is

$$\begin{aligned} \delta\mathbf{u}(\mathbf{r}_r, t) \cdot \mathbf{v} &= -\int_V \mathbf{d}(\mathbf{r})\, d\mathbf{r} \\ &\simeq -\sum_{e=1}^{N_e} \sum_{i,j,k} \mathbf{d}(\mathbf{r}_{ijk}) |\mathcal{J}^e(\boldsymbol{\xi}_{ijk}) \rho_i^N \rho_j^N \rho_k^N \,, \end{aligned} \tag{23}$$

where $\mathbf{r} = \mathcal{F}_e(\boldsymbol{\xi})$ with $\mathcal{F}_e$ the transformation function from the reference cube to the deformed cube number e, $\mathcal{J}^e$ the Jacobian of the transformation $\mathcal{F}_e$ and ρ_i^N the 1-D integration weights associated with GLL point number i among $N + 1$. For more details about the integration scheme we refer to Komatitsch & Vilotte (1998) and Chaljub *et al.* (2003). Our experience with spectral elements and with the method presented here shows that a good accuracy is achieved with two minimum wavelength per element of degree 8. This sampling may need to be increased in some cases like a sharp variation of the elastic property within an element. Discontinuities of elastic properties or eigenfunction derivatives are accurately integrated only if they match element interfaces.

In this paper, the integration is performed as explained above by computing $\mathbf{d}(\mathbf{r})$ for every scattering point of the integration mesh but heavy computational optimization can be performed here. First, not all scattering points contribute significantly to $\delta\mathbf{u}$. Indeed, the sensitivity of a wave for a given source and receiver configuration is primarily focused on the Fresnel zone and this can be used to reduce computations. Second, as proposed by Zhao & Chevrot (2004), a 2-D mesh of 1-D Green's functions can be computed and stored and finally used to compute the contribution of all the required integration points using interpolations. Indeed, each component of eqs (12) and (13) or (A11) and (A12) only depends on the source depth and an epicentral distance (between the source and the integration point or between the integration point and the receiver). Therefore, all the terms can be pre-computed on a 2-D mesh with a good spacial sampling rate and stored in a database. Some elements of the database will be later loaded to compute eq. (11) for a particular source–receiver configuration.This solution requires some heavy bookkeeping, but this is probably necessary to be effective when dealing with higher frequencies and body waves to compute a large number of kernels.

3.3 Frechet derivatives

So far we have discussed solutions for a single model perturbation $\delta\boldsymbol{\mathcal{L}}$, which is typically the case when computing synthetic

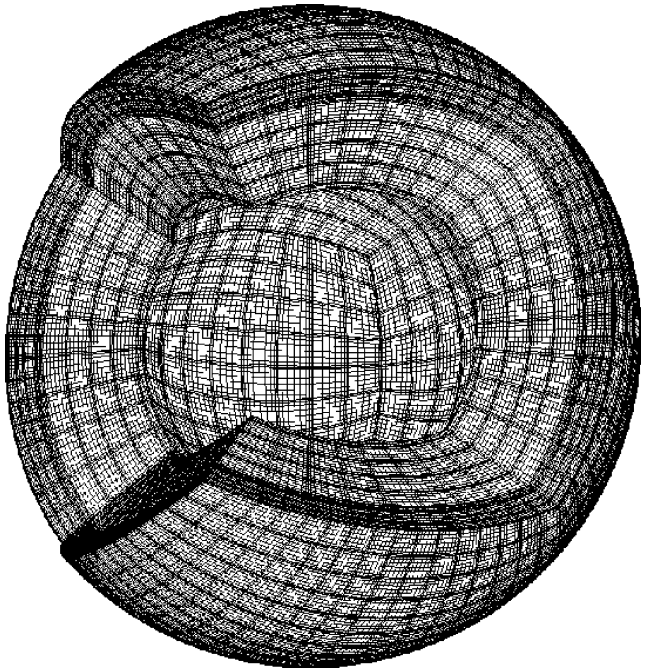

Figure 4. Typical integration mesh used for the volume integration of eq. (11). Two regions of the cubic sphere have been removed for this figure for representation purpose.

seismograms. When dealing with Frechet derivatives, the solution $\delta\mathbf{u}$ has to be computed for each spatial parameter p of the parametrization used in the inversion process. Each parameter p can be either global as a spherical harmonic or local as a spherical spline. For the sake of simplicity, let us say that we are working with a single elastic parameter (e.g. V_s) and let $\delta\boldsymbol{\mathcal{L}}_1$ be the unit perturbation operator for which this single elastic parameter is 1 everywhere. We name $p(\mathbf{r})$ the spacial variation of the elastic parameter corresponding to p, then the perturbation of the elastic operator for the parameter p is $\delta\boldsymbol{\mathcal{L}}_p(\mathbf{r}) = p(\mathbf{r})\delta\boldsymbol{\mathcal{L}}_1$. We, therefore, have

$$\frac{\partial \mathbf{u}(\mathbf{r}_r, t)}{\partial p} \cdot \mathbf{v} = -\sum_{e=1}^{N_e} \sum_{i,j,k} p(\mathbf{r}_{ijk}) \mathbf{d}_1(\mathbf{r}_{ijk}) |\mathcal{J}^e(\boldsymbol{\xi}_{ijk})| \rho_i^N \rho_j^N \rho_k^N \,, \quad (24)$$

where

$$\mathbf{d}_1(\mathbf{r}) = \int \mathbf{B}(\mathbf{r}, \tau) \cdot \delta\boldsymbol{\mathcal{L}}_1(\mathbf{r}) \mathbf{F}(\mathbf{r}, \tau - t)\, d\tau \,. \quad (25)$$

In practice, computing $\mathbf{d}_1(\mathbf{r}_{ijk})$ represents most of the CPU time required for the whole computation, and, as they are common to all the parameter p, they need to be computed only once. This makes the computation of all the Frechet derivatives independent of their number. Of course, this technique can be used to compute different type of kernels (time arrivals, phase velocity, etc.).

4 VALIDATIONS

In order to test and validate this work, we will compare results obtained with this Born solution and the one obtained by the SEM. More specifically, we will use the coupled SEM–normal mode method (Chaljub *et al.* 2003; Capdeville *et al.* 2003): the SEM will be used in the mantle and the normal mode solution in the core, which will remain spherically symmetric. Both of these methods contain approximations and, therefore, none of them can be considered as an absolute reference with respect to the other one. Nevertheless, as the solutions used to solve the wave equation in both cases are completely different, there is a good chance that both solutions are correct if the two solutions match. We first performed a validation test in the Frechet kernel case. We define a single and simple spatial parameter p: a vertical cylinder of 10° of diameter from the surface to the 660 km transition zone. The amplitude on the elastic parameter contrast in the cylinder has a Gaussian shape. To compute the full waveform partial derivative with respect to this cylindrical spatial parameter p with SEM, we use a simple finite difference formula:

$$\frac{\partial \mathbf{g}(0)}{\partial p} \simeq \frac{\mathbf{g}(\delta p) - \mathbf{g}(0)}{\delta p} \,, \quad (26)$$

where $\mathbf{g}(\delta p)$ represent the waveform at a given seismic station computed with SEM in the earth model PREM plus δp. In practice we perform two SEM runs, one in the reference model (PREM) and one in the 3-D model built with PREM plus a 3-D structure of shape p and a small amplitude, and then take the difference. In that test, anelasticity is turned off. Fig. 5 presents a comparison of SEM and normal modes results for two elastic parameters, $\delta\Lambda^{0000}$ and the real part of $\delta\Lambda^{++00}$ (see eq. A2). The agreement between the two methods is very good.

The second test is performed in the tomographic model SAW24B16 for the source–receiver locations presented in Fig. 6. SAW24B16 is a V_s model and, for this test V_p and ρ perturbations

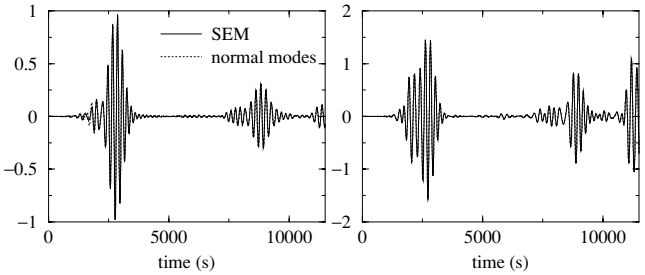

Figure 5. Examples of partial derivatives waveforms (vertical component) with respect to the cylindrical structure p computed with SEM (solid line) and the normal modes Born algorithm presented in this paper (dotted line), for elastic parameter $\delta\Lambda^{0000}$ (left plot) and the real part of $\delta\Lambda^{++00}$ (right plot). The source corner frequency is 150 s and at 19 km depth, the receiver is at an epicentral distances of 90° and the cylinder p is on the great circle path and at the same distance from the source and the receiver.

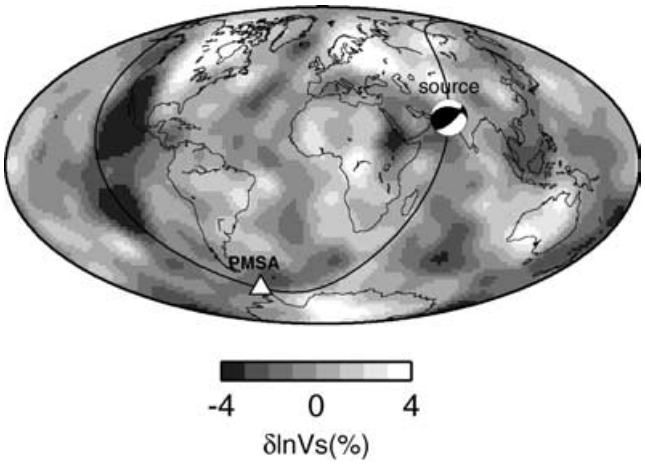

Figure 6. Source station path used for the test performed in SAW24B16 tomographic model. The source is at 19 km depth. The background map represents SAW24B16 velocity perturbations at 200 km depth.

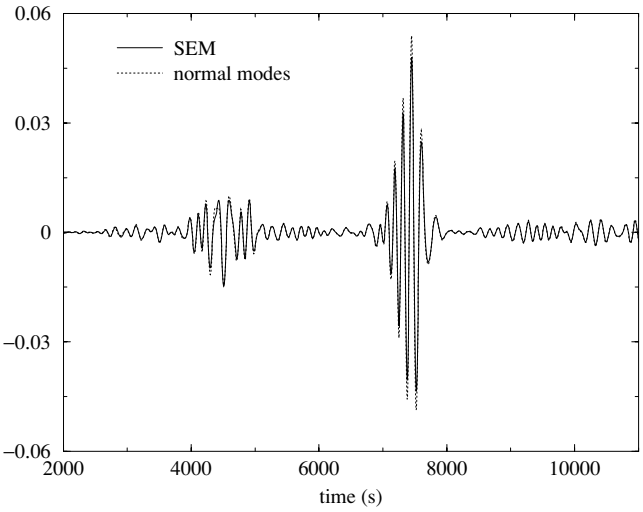

Figure 7. Differential waveforms computed by SEM (solid line) and by the normal modes perturbation technique presented in this paper (dotted line). The source–receiver configuration is given Fig. 6. The model is SAW24B16 with an amplitude of velocity contrast divided by 10 to avoid most of the non-linear effects. The corner period of the source is here 100 s.

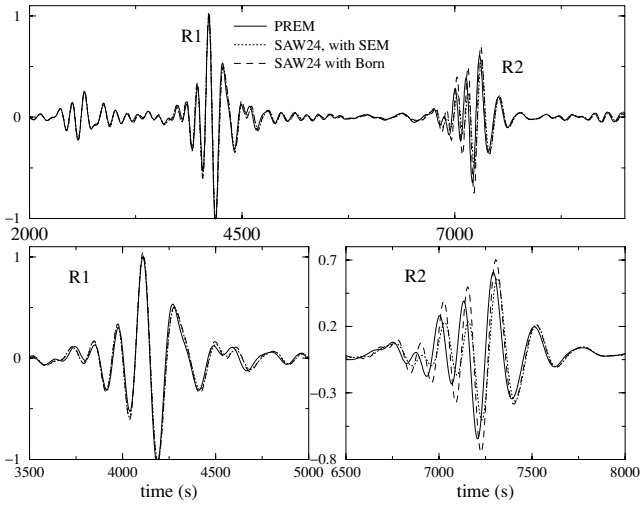

Figure 8. Top: Vertical component synthetic waveforms computed in PREM (solid line), SAW24B16 with SEM (dotted line) and in SAW24B16 within the Born approximation (dashed line) for the same source–receiver configuration as in Fig. 7. The two lower plots are zooms on R1 and R2 phases of the same seismograms. Non-linear effects are significant on R2. The differences between SEM and normal modes computation observed in Fig. 7 are small compared to the non-linear differences observed here.

have been linearly linked to V_s. In order to avoid most of the non-linear effects that will be present in the SEM simulation we first perform a run in a SAW24B16 model with an amplitude of velocity contrasts divided by 10. The result is presented in Fig. 7. The agreement is good, but not perfect for the amplitudes. This difference can be accounted for by the difference in the attenuation scheme. When we use SAW24B16 with its real amplitude, non-linear effects become important as can seen in Fig. 8, especially for the R2 Rayleigh phase, even for these long period (100 s and above). The conclusion of this last test is that, when using Born to compute synthetic seismograms, non-linear effects can be important and it should be checked if this approximation is valid, even at long periods when long time-series (e.g. R2) are used. Of course, this is not a concern when building partial derivatives.

5 DISCUSSION AND CONCLUSIONS

We have presented a solution to compute synthetic seismograms in 3-D global models earth and Frechet partial derivatives for global tomography based on the Born approximation in the normal mode framework. The main interest of this solution is to reduce the number of computations with respect to classical approaches by avoiding to explicitly have to compute the mode coupling due to the presence of lateral heterogeneities. Indeed, the numerical cost of the scheme proposed here grows as (number of receivers + the number of sources) × (corner frequency)^2 to be compared to (number of receivers × the number of sources) × (corner frequency)^4 when the classical normal mode coupling algorithm is used. This approach, which involves the convolution of direct wavefield form the source to a scattering point with a backward wavefield from the receiver to the scattering point, is very similar to adjoint problem approaches used to compute the gradient in seismic inverse problem (Lailly 1983; Tarantola 1984, 1988; Mora 1987; Geller & Hara 1993; Pratt *et al.* 1998; Tromp *et al.* 2005). The CPU time required for this approach as presented here can be significantly improved by storing 2-D propagation functions and then use interpolations to compute the direct and backward wavefield at the different scattering points of the 3-D integration mesh as proposed by Zhao & Chevrot (2004). This improvement can be very useful especially if the scheme is used to compute time arrival kernels for body waves, which require high frequencies and therefore a large number of modes.

Our comparison with the SEM have shown a good agreement for the Frechet derivatives case. When used to compute synthetic seismograms, differences can be significant, even in a long period and in smooth 3-D models. These differences are due to non-linear effects and have, therefore, less to do with the scheme used than with the Born approximation. It should be noted anyway that there is still one drawback to this technique in that case. Indeed, classical mode coupling calculations allow to correct eigenfrequencies as explained by Woodhouse (1983), which allow to perform some approximate non-linear correction. This cannot be done with the method presented here. Finally, one should always worry about non-linear effect especially when working on R2 or long epicentral distance R1 phase velocities and amplitudes, even at long periods.

Applications of this work should be found for the computation of different type of Frechet kernels from time arrival kernels to full waveform kernels for global earth tomography.

ACKNOWLEDGMENTS

I thank Paco Sánchez–Sesma for a fruitful discussion which indirectly initiated this work. I also thank Barbara Romanowicz for many interesting discussions about this topic. Finally I thank two anonymous reviewers for helping to improve the manuscript. Computations were performed with IDRIS, CINES and IPGP IBM computer facilities.

REFERENCES

Capdeville, Y., Chaljub, E., Vilotte, J.P. & Montagner, J.P., 2003. Coupling the spectral element method with a modal solution for elastic wave propgation in global earth models, *Geophys. J. Int.,* **152,** 34–66.

Capdeville, Y., Stutzmann, E. & Montagner, J.P., 2000. Effect of a plume on long period surface waves computed with normal modes coupling, *Phys. Earth Planet. Inter.,* **119,** 57–74.

Chaljub, E., 2000. Modèlisation numérique de la propagation d'ondes sismiques à l'échelle du globe. *Thèse de doctorat* de l'Université Paris 7.

Chaljub, E., Capdeville, Y. & Vilotte, J.P., 2003. Solving elastodynamics in a fluid-solid heterogeneous sphere: a spectral element approximation on geometrically non-conforming grids, *J. Comp. Physics*, **187,** 457–491.

Dziewonski, A.M. & Anderson, D.L., 1981. Preliminary reference Earth model, *Phys. Earth Planet. Inter.,* **25,** 297–356.

Edmonds, A.R., 1960. *Angular Momentum and Quantum Mechanics*. Princeton University Press, New Jersey.

Geller, R.J. & Hara, T., 1993. Two efficient algorithms for iterative linearized inversion of seismic waveform data, *Geophys. J. Int.,* **115,** 699–710.

Komatitsch, D. & Vilotte, J.P., 1998. The spectral element method: an effective tool to simulate the seismic response of 2d and 3d geological structures, *Bull. Seism. Soc. Am.,* **88,** 368–392.

Lailly, P., 1983. The seismic inverse problem as a sequence of before stack migrations. In J. Bednar, R., Redner, E. Robinson, & A. Weglein (Eds.), *Conference on Inverse Scattering: Theory and Application*. Soc. Industr. appl. Math., Philadelohia, Pennsylvania.

Li, X.D. & Romanowicz, B., 1995. Comparison of global waveform inversions with and without considering cross–branch modal coupling, *Geophys. J. Int.,* **121,** 695–709.

Li, X.D. & Tanimoto, T., 1993. Waveforms of long–period body waves in slightly aspherical Earth model, *Geophys. J. Int.,* **112,** 92–102.

Mégnin, C. & Romanowicz, B., 2000. The 3-D shear velocity structure of the mantle from the inversion of body, surface and higher modes wave forms, *Geophys. J. Int.,* **143,** 709–728.

Mora, P., 1987. Nonlinear two-dimensional elastic inversion of multioffset seismic data, *Geophysics* **52**(9), 1211–1228.

Phinney, R.A. & Burridge, R., 1973. Representation of elastic-gravitational excitation of a spherical earth model by generalized spherical harmonics, *Geophys. J. R. Astron. Soc.,* **34,** 451–278.

Pratt, R., Shin, C. & Hicks, G., 1998. Gauss-newton and full newton methods in frequency domain seismic waveform inversion, *Geophys. J. Int.,* **133,** 341–362.

Romanowicz, B., 1987. Multiplet–multiplet coupling due to lateral heterogeneity: asymptotic effects on the amplitude and frequency of the Earth's normal modes, *Geophys. J. R. Astron. Soc.,* **90,** 75–100.

Ronchi, C., Ianoco, R. & Paolucci, P.S., 1996. The 'Cubed Sphere': a new method for the solution of partial differential equations in spherical geometry, *J. Comput. Phys.,* **124,** 93–114.

Sadourny, R., 1972. Conservative finite-difference approximations of the primitive equation on quasi-uniform spherical grids, *Mon. Weather Rev.,* **100,** 136–144.

Snieder, R., 1986. 3-D Linearized scattering of surface waves and formalism for surface wave holography, *Geophys. J. R. Astron. Soc.,* **84,** 581–605.

Snieder, R. & Romanowicz, B., 1988. A new formalis for the effect of lateral heterogeneity on normal modes and surface waves: I. Isotropic perturbations, perturbations of interfaces and gravitational perturbances, *Geophys. J. Int.,* **92,** 207–222.

Tanimoto, T., 1984. A simple derivation of the formula to calculate synthetic long period seismograms in heterogeneous earth by normal mode summation, *Geophys. J. R. Astron. Soc.,* **77,** 275–278.

Tanimoto, T., 1986. Free oscillations of a slightly anisotopic earth, *Geophys. J. R. Astron. Soc.,* **87,** 493–517.

Tanimoto, T., 1990. Modelling curved surface wave paths: membrane surface wave synthetics, *Geophys. J. Int.,* **102,** 89–100.

Tarantola, A., 1984. Inversion of seismic reflection data in the acoustic approximation, *Geophysics*, **49,** 1259–1266.

Tarantola, A., 1988. Theoritical background for the inversion of seismic waveforms, including elasticity and attenuation, *Pure Appl. Geophys*. **128**(1/2), 365–399.

Tromp, J., Tape, C. & Liu, Q., 2005. Seismic tomography, adjoint methods, time reversal and banana-doughnut kernels, *Geophys. J. Int.*, **160,** 195–216.

Woodhouse, J., 1983. The joint inversion of seismic wave forms for lateral variations in Earth structure and earthquake source parameter. In *Physics of the Earth's Interior*, Volume 85, Amsterdam, pp. 366–397. Int. School of Physics 'Enrico Fermi', North-Holland.

Woodhouse, J.H. & Dahlen, F.A., 1978. The effect of a general aspherical perturbation on the free oscillations of the Earth, *Geophys. J. R. Astron. Soc.,* **53,** 335–354.

Woodhouse, J.H. & Dziewonski, A.M., 1984. Mapping the upper mantle: three–dimensional modeling of earth structure by inversion of seismic waveforms, *J. Geophys. Res.,* **89,** 5953–5986.

Woodhouse, J.H. & Girnius, T.P., 1982. Surface waves and free oscillations in a regionalized earth model, *Geophys. J. R. Astron. Soc.,* **78,** 641–660.

Zhao, L. & Chevrot, S., 2004. Three-dimensional full-wave tomography on a laptop. In *Eos Trans. AGU*, Volume 85 (47). Fall meet. Suppl., Abstract S53B-0225.

APPENDIX A: PRACTICAL EXPRESSIONS

Considering only a perturbation of the anelastic tensor $\delta\mathbf{c}$ and using an integration by part, eq. (10) can be rewritten

$$\delta\mathbf{u}(\mathbf{r}_r,\omega)\cdot\mathbf{v} = \int_V \left[\sum_K \frac{\boldsymbol{\epsilon}_K^*(\mathbf{r})R_K}{(\omega_k^2-\omega^2)}\right] : \delta\mathbf{c}(\mathbf{r}_d) : \left[\sum_K \frac{\boldsymbol{\epsilon}_K(\mathbf{r})S_K}{i\omega(\omega_k^2-\omega^2)}\right] d\mathbf{r}_d, \tag{A1}$$

where $\boldsymbol{\epsilon}_K$ the deformation tensor corresponding to the mode $\mathbf{u}_K$. In the following, generalized spherical harmonics expansion will be used to simplify expressions. To do so, it is useful to use the contravariant canonical component of $\delta\mathbf{c}$

$$\delta\Lambda^{\alpha\beta\gamma\eta} = \sum_{ijkl} C^\star_{\alpha i}C^\star_{\beta j}C^\star_{\gamma k}C^\star_{\eta l}\delta c_{ijkl}\,, \tag{A2}$$

as well as for the deformation tensor associated to mode $\mathbf{u}_K$

$$\epsilon_K^{\alpha\beta}(\mathbf{r}) = \sum_{ij} C^\star_{\alpha i}C^\star_{\beta j}\epsilon_{K,ij}(\mathbf{r}), \tag{A3}$$

where $\mathbf{C}$ is

$$(C_{i\alpha}) = \begin{pmatrix} 0 & 1 & 0 \\ \frac{1}{\sqrt{2}} & 0 & \frac{-1}{\sqrt{2}} \\ \frac{1}{\sqrt{2}} & 0 & \frac{-i}{\sqrt{2}} \end{pmatrix}. \tag{A4}$$

Generalized spherical harmonics expansion of R_K, S_K and $\epsilon_K^{\alpha\beta}$ are well known:

$$R_K(\mathbf{r}_r) = \sum_{\alpha=-1,1} R_k^{\alpha}(r_r) Y_l^{\alpha m}(\theta_r, \phi_r)\,, \tag{A5}$$

$$S_K(\mathbf{r}_s) = \sum_{\alpha=-2,2} S_k^{\alpha}(r_s) Y_l^{\alpha m\star}(\theta_s, \phi_s)\,, \tag{A6}$$

$$\epsilon_K^{\alpha\beta}(\mathbf{r}_d) = E_k^{\alpha\beta}(r_d) Y_l^{\alpha+\beta\ m}(\theta_d, \phi_d), \tag{A7}$$

where $Y_l^{\alpha m}$ is the generalized spherical harmonics, the expression of R_k^{α} and S_k^{α} can be found in Woodhouse & Girnius (1982) and where $E_k^{\alpha\beta}$ can be easily evaluated and can be found, for example, in Tanimoto (1986). We define

$${}_b\mathbf{E}(\mathbf{r}_d, \omega) = \sum_K \frac{\boldsymbol{\epsilon}_K^{\star}(\mathbf{r}_d) R_K}{\left(\omega_k^2 - \omega^2\right)}, \tag{A8}$$

which in the time domain and with canonical component gives

$${}_bE^{\alpha\beta}(\mathbf{r}_d, t) = \sum_{K\eta} R_k^{\eta} E_k^{\alpha\beta\star}(r) Y_l^{\eta m}(\theta_r, \phi_r) Y_l^{\alpha+\beta\ m}(\theta, \phi) \frac{\sin(\omega_k t)}{\omega_k} H(t). \tag{A9}$$

At this point, the spherical harmonics summation theorem is useful to suppress the sum over m. We have (Li & Tanimoto 1993):

$$\sum_{m=-l}^{m=l} Y_l^{N'm\star}(\theta_s, \phi_s) Y_l^{Nm}(\theta_r, \phi_r) = e^{iN'\gamma_{sr}} P_l^{NN'}(\cos(\beta_{sr})) e^{iN\xi_{sr}}\,, \tag{A10}$$

where $P_l^{NN'}$ are the generalized Legendre functions. If the index s is related to the 'source' location and r to the 'receiver' one, then the angle $-\xi_{sr}$ is the backazimuth at the receiver, $\pi - \gamma_{sr}$ the azimuth at the source and β_{sr} is the angular epicentral distance. Using this theorem, eq. (A9) becomes

$${}_bE^{\alpha\beta}(\mathbf{r}_d, t) = \sum_{k\eta} R_k^{\eta}\, E_k^{\alpha\beta\star}(r_d)\, P_l^{\eta\ \alpha+\beta}(\cos(\beta_{rd}))\, e^{i(\alpha+\beta)\gamma_{dr} + i\eta\xi_{dr}}\ \frac{\sin(\omega_k t)}{\omega_k} H(t). \tag{A11}$$

Similarly, we define

$${}_fE^{\alpha\beta}(\mathbf{r}_d, t) = \sum_{k\eta} S_k^{\eta}\, E_k^{\alpha\beta}(r_d)\, P_l^{\alpha+\beta\ \eta}(\cos(\beta_{sd}))\, e^{i(\alpha+\beta)\xi_{sd} + i\eta\gamma_{dr}}\ \frac{1-\cos(\omega_k t)}{\omega_k^2} H(t). \tag{A12}$$

Finally, knowing that $\sum_i C_{i\alpha}^{\star} C_{i\beta} = \delta_{\alpha\beta}$ and $\sum_i C_{i\alpha} C_{i\beta} = e_{\alpha\beta}$ with

$$(e_{\alpha\beta}) = \begin{pmatrix} 0 & 0 & -1 \\ 0 & 1 & 0 \\ -1 & 0 & 0 \end{pmatrix}. \tag{A13}$$

Eq. (A1) gives

$$\delta\mathbf{u}(\mathbf{r}_r, \omega)\cdot\mathbf{v} = \int_V \int \sum_{\alpha\beta\gamma\eta\iota\kappa} {}_bE^{\alpha\beta}(\mathbf{r}_d, \tau)\delta\Lambda^{\alpha\beta\gamma\eta}(\mathbf{r}_d)\, {}_fE^{\iota\kappa}(\mathbf{r}_d, t-\tau) e_{\gamma\iota} e_{\eta\kappa}\, d\tau d\mathbf{r}_d\,. \tag{A14}$$

For a density perturbation, using the following generalized spherical harmonic expansion for the eigendisplacement,

$$\mathbf{U}_K^{\alpha}(\mathbf{r}_d) = U_k^{\alpha}(r_d) Y_l^{\alpha\ m}(\theta_d, \phi_d)\,, \tag{A15}$$

and defining

$${}_bU^{\alpha}(\mathbf{r}_d, t) = \sum_{k\eta} R_k^{\eta}\, U_k^{\alpha\star}(r_d)\, P_l^{\eta\ \alpha}(\cos(\beta_{rd}))\, e^{i\alpha\gamma_{dr} + i\eta\xi_{dr}}\ \sin(\omega_k t)\omega_k H(t)\,, \tag{A16}$$

$${}_fU^{\alpha}(\mathbf{r}_d, t) = \sum_{k\eta} S_k^{\eta}\, U_k^{\alpha}(r_d)\, P_l^{\alpha\ \eta}(\cos(\beta_{sd}))\, e^{i\alpha\xi_{sd} + i\eta\gamma_{dr}}\ \frac{1-\cos(\omega_k t)}{\omega_k^2} H(t)\,, \tag{A17}$$

the displacement perturbation is

$$\delta\mathbf{u}(\mathbf{r}_r, \omega)\cdot\mathbf{v} = -\int_V \delta\rho(\mathbf{r}_d) \sum_{\alpha} \int {}_bU^{\alpha}(\mathbf{r}_d, \tau)\, {}_fU^{\alpha}(\mathbf{r}_d, t-\tau)\, d\tau d\mathbf{r}_d\,. \tag{A18}$$